EJPMR, 2026, 13(11), 674-682 **Research Article** **Impact Factor: 8.158**

EUROPEAN JOURNAL OF PHARMACEUTICAL AND MEDICAL RESEARCH

www.ejpmr.com

ISSN (O): 2394-3211
ISSN (P): 3051-2573
Coden USA:EJPMAG

EFFICIENT GRAPHENE OXIDE-CATALYZED MULTICOMPONENT SYNTHESIS OF TETRAHYDROBENZO[A]XANTHEN-11-ONE DERIVATIVES WITH MOLECULAR DOCKING STUDIES

Kagane Priyanka[1], S. Santosh Kumar[1], Jadhav Tejaswita[1], Kamble Rohini[1], Kalalawe Virbhadra[1*]

[1]Department of Chemistry, Yogeshwari Mahavidyalaya Ambajogai, Ambajogai-431517.

***Corresponding Author: Kalalawe Virbhadra**

Department of Chemistry, Yogeshwari Mahavidyalaya Ambajogai, Ambajogai-431517.

DOI: https://doi.org/10.5281/zenodo.24463744

How to cite this Article: Kagane Priyanka[1], S. Santosh Kumar[1], Jadhav Tejaswita[1], Kamble Rohini[1], Kalalawe Virbhadra[1]*. (2026). Efficient Graphene Oxide-Catalyzed Multicomponent Synthesis of Tetrahydrobenzo[a]xanthen-11-one Derivatives with Molecular Docking Studies. European Journal of Pharmaceutical and Medical Research, 13(11), 674–682.
This work is licensed under Creative Commons Attribution 4.0 I nternational license.

Article Received on 05/10/2026 **Article Revised on 25/10/2026** **Article Published on 01/11/2026**

ABSTRACT

A simple and green method for the synthesis of xanthene derivatives has been developed via a one-pot multicomponent reaction of aromatic aldehydes, β-naphthol, and dimedone using graphene oxide as an efficient heterogeneous catalyst in ethanol. The protocol affords the desired products in good to excellent yields under mild conditions with a simple work-up procedure. The use of recyclable graphene oxide and ethanol as a green solvent makes this approach an efficient and environmentally friendly alternative for the synthesis of biologically important xanthene derivatives.

KEYWORDS: Xanthene derivatives; Graphene oxide; Multicomponent reaction; Heterogeneous catalyst; Green synthesis; Dimedone; β-Naphthol; Aromatic aldehydes; Ethanol; One-pot synthesis.

1. INTRODUCTION

Xanthene derivatives constitute an important class of oxygen-containing heterocyclic compounds that have attracted considerable attention because of their broad range of biological and technological applications. Members of this structural family have been reported to exhibit antibacterial.[1] anti-inflammatory,[2] and antiviral.[3] activities. In addition, their pH-responsive fluorescent properties have enabled applications in the imaging of biomolecular assemblies,[4] while xanthene-based frameworks are also widely associated with dyes.[5-6] & laser technology.[7-8] Consequently, the development of efficient and sustainable synthetic routes to structurally diverse xanthene derivatives remains an important area of research in organic and medicinal chemistry.

Multicomponent reactions (MCRs) have emerged as powerful synthetic tools for the rapid construction of complex molecular frameworks. In these reactions, three or more readily available starting materials are combined in a single reaction vessel to generate the desired product without the isolation of intermediates. Such one-pot strategies offer important advantages, including improved atom economy, reduced purification steps, operational simplicity, and decreased generation of chemical waste. These characteristics make MCRs particularly attractive for the synthesis of heterocyclic compounds, including biologically relevant xanthene scaffolds.

Several catalytic methods have been reported for the synthesis of xanthene derivatives using I_2[9] guanidine-HCl,[10] CA–SiO_2,[11] $HClO_4$–SiO_2,[12] PWA,[13] TCT,[14] $InCl_3$,[15] strontium triflate,[16] surfactants,[17] SaSA,[18] and tungstosilicic acid[19]. Although these procedures have contributed significantly to the development of xanthene chemistry, some methodologies involve relatively harsh reaction conditions, prolonged reaction times, corrosive or hazardous catalysts, toxic reaction media, difficult product isolation, or limited catalyst recovery. Therefore, the search for environmentally compatible, metal-free, and heterogeneous catalytic systems remains highly desirable. Recent developments in xanthene synthesis and graphene-based catalytic materials further highlight the growing interest in sustainable catalytic approaches.[20–22]

Graphene oxide (GO) has emerged as a promising metal-free heterogeneous carbocatalyst for organic transformations because of its two-dimensional structure, large specific surface area, and the presence of abundant oxygen-containing functional groups, including hydroxyl, epoxy, carbonyl, and carboxyl functionalities. These surface groups can provide acidic and other catalytic sites, while the heterogeneous nature of GO facilitates catalyst separation and offers the possibility of recovery and reuse. The versatility of GO and functionalized GO in catalytic organic transformations and heterocyclic synthesis has been increasingly recognized.[23]

2. MATERIALS AND METHODS

All chemicals and reagents were procured from Sigma-Aldrich and Spectrochem and used without further purification unless otherwise stated. Melting points were determined using the open-capillary method and are reported without correction. The ^{1}H NMR spectra were recorded at room temperature on a Bruker Avance II 400 MHz spectrometer (SAIF, Panjab University, Chandigarh) using $CDCl_3$ as the solvent and tetramethylsilane (TMS) as the internal reference. FTIR spectra were obtained from KBr pellets using a PerkinElmer Spectrum RX FTIR spectrometer (SAIF, Panjab University, Chandigarh, India). Reaction progress was monitored by thin-layer chromatography (TLC) using precoated silica gel plates on aluminium sheets (Merck).

General procedure for the synthesis of Graphene oxide

Graphene oxide (GO) was synthesized from graphite powder using a modified Hummers method[24] Briefly, graphite powder (2.5 g) and sodium nitrate ($NaNO_3$, 1.25 g) were added to concentrated sulfuric acid (H_2SO_4, 57.5 mL) under ice-bath cooling. Potassium permanganate ($KMnO_4$, 7.5 g) was then added gradually with continuous stirring, while maintaining the temperature below 20 °C. The resulting mixture was stirred under ice-bath conditions for 30 min and subsequently heated in a water bath at 40 °C for 40 min. Afterward, 100 mL of hot water was carefully added, followed by the addition of 25 mL of hydrogen peroxide solution (25 wt%) to terminate the oxidation process. The resulting suspension was filtered and thoroughly washed several times with deionized water to remove residual acid and inorganic salts. Finally, the obtained graphene oxide was dried in a hot-air oven at 60 °C and used for further characterization and catalytic studies.

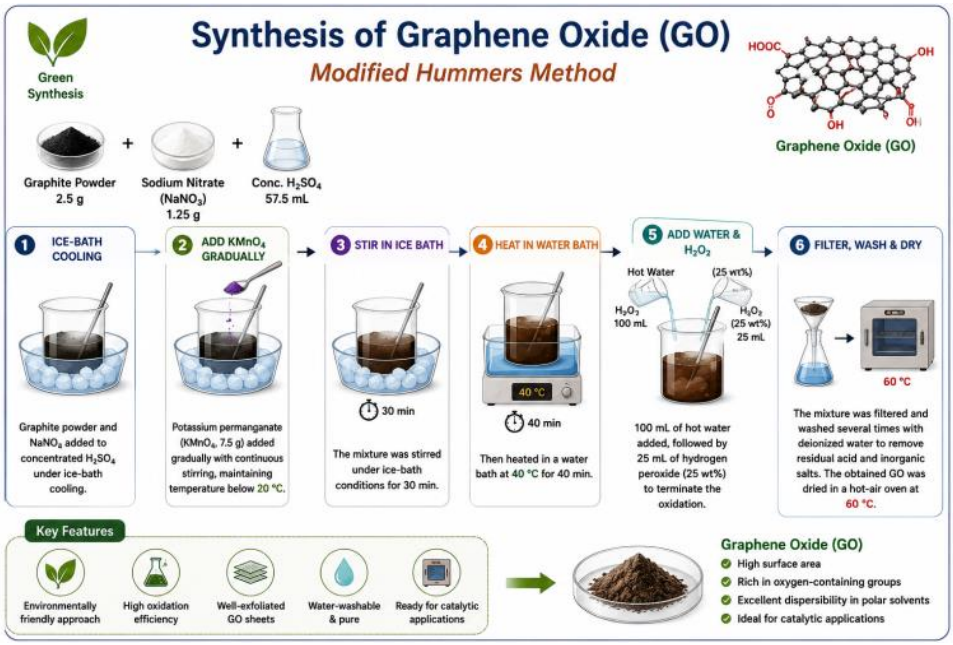

Scheme 1: Preparation of Graphene oxide.

The structural and surface characteristics of the synthesized graphene oxide (GO) were investigated using FT-IR spectroscopy, X-ray diffraction (XRD), and field-emission scanning electron microscopy (FESEM). The FT-IR spectrum (Fig.1) displays the characteristic absorption bands associated with the oxygen-containing functional groups present on the GO surface. The broad absorption band centered at approximately 3350 cm^{-1} can be assigned to the O–H stretching vibration of hydroxyl groups. The bands observed around 1735 cm^{-1} are attributed to the C=O stretching vibration of carbonyl/carboxyl groups. In addition, the absorptions at approximately 1224 and 1053 cm^{-1} can be assigned to C–O stretching vibrations associated with epoxy and other oxygen-containing functionalities. These characteristic bands confirm the successful oxidation and functionalization of the graphitic framework.

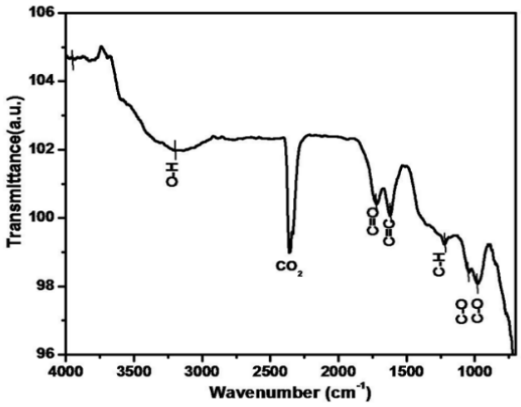

Fig. 1: IR of graphene oxide.

The crystalline characteristics of the prepared GO were examined by XRD (Fig. 2). A prominent diffraction peak corresponding to the (002) plane was observed at approximately 2θ = 10.84°, indicating the formation of graphene oxide. Using Bragg's equation, $n\lambda = 2d \sin \theta$, where λ = 0.154 nm, the calculated interlayer distance was approximately 0.82 nm. This value is substantially larger than the characteristic interlayer spacing of pristine graphite (~0.337 nm). The increase in interlayer distance can be attributed to the incorporation of oxygen-containing functional groups, together with intercalated water molecules, during the oxidation of graphite. These functionalities increase the separation between adjacent graphene layers and provide abundant surface-active sites, which are beneficial for heterogeneous catalysis.

The surface morphology of the prepared GO was further investigated by FESEM (Fig. 3). The micrographs reveal a characteristic lamellar and wrinkled layered morphology, with interconnected sheets forming an extended porous surface. The observed nanosheet architecture provides a relatively high accessible surface area and numerous exposed functional groups, which can facilitate interactions between the catalyst and reactant molecules. The morphological features, together with the FT-IR and XRD results, provide complementary evidence for the successful formation of graphene oxide and support its application as a heterogeneous catalyst in the present multicomponent synthesis.

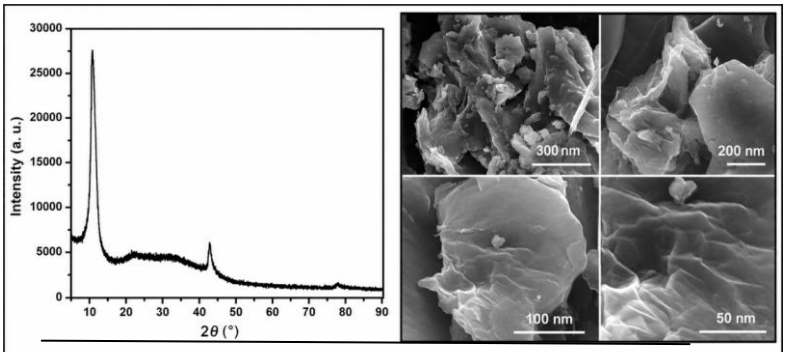

Fig 2: XRD of Graphene Oxide **Fig 3: FESEM of Graphene Oxide**

3. Experimental

A mixture of β-naphthol (1 mmol), dimedone (1 mmol), an aromatic aldehyde (1 mmol), and graphene oxide (25 mol%) in ethanol was placed in a 50 mL round-bottom flask and heated under reflux for the required reaction time. The progress of the reaction was monitored by TLC. Upon completion, as indicated by TLC, the reaction mixture was allowed to cool to room temperature. The catalyst was separated from the reaction mixture by filtration, and the solvent was removed under reduced pressure. The resulting crude product was purified by recrystallization from ethanol (96%) to afford the corresponding xanthene derivative in pure form.

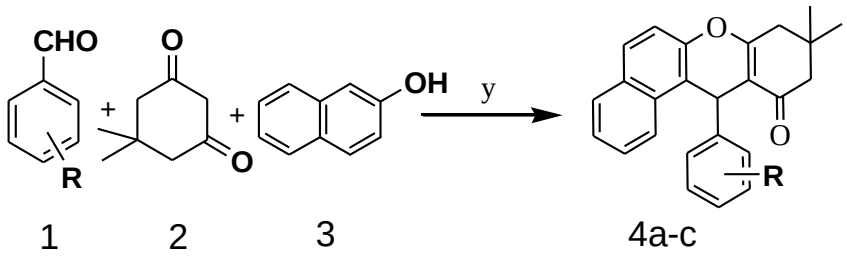

Reagent and condition: y) Graphene Oxide, Ethanol, Reflux, 1-2 Hrs, 80-97% yields.

4. RESULTS AND DISCUSSION

The development of efficient and sustainable catalytic protocols for multicomponent organic synthesis remains an important objective in contemporary synthetic chemistry. In the present study, graphene oxide (GO) was investigated as a heterogeneous and environmentally benign catalyst for the one-pot three-component synthesis of xanthene derivatives using β-naphthol, dimedone, and substituted aromatic aldehydes in ethanol under reflux conditions. Initially, the three-component reaction of β-naphthol (1 mmol), dimedone (1 mmol), and 3-nitro benzaldehyde (1 mmol) was selected as a model reaction to investigate the catalytic performance of graphene oxide and establish suitable reaction conditions. The influence of different reaction media on the formation of 9,9-dimethyl-9,10-dihydro-12-(3-nitrophenyl)-8H-benzo[a]xanthen-11(12H)-one was first examined in the presence of graphene oxide under reflux conditions. Among the solvents screened, ethanol proved to be the most effective reaction medium, affording the desired product in excellent yield within a comparatively shorter reaction time (Table 1). Therefore, ethanol was selected as the preferred solvent for subsequent optimization studies.

Table 1: Solvent optimization for synthesis of Xanthene derivatives. using Graphene Oxide.

Entry	Solvent	Time (h)	Yield[b] (%)
1	No solvent	5	00
2	Toluene	4	68
3	Acetonitrile	3.5	71
4	Chloroform	3.3	75
5	DMF	3.2	78
6	Methanol	2.0	89
7	Ethanol	2.0	91

[a]Reaction condition: 3-nitro benzaldehyde (1mmol), ethyl, β-naphthol (1mmol), dimedone (1mmol) and various solvents using Graphene Oxide catalyst at various temperature. [b]Isolated Yield After establishing ethanol as the most suitable reaction medium, the effect of graphene oxide loading on the model reaction was investigated. The three-component reaction of β-naphthol (1 mmol), dimedone (1 mmol), and 3-nitro benzaldehyde (1 mmol) was carried out in refluxing ethanol using different amounts of graphene oxide (Table 2). The results revealed that the reaction efficiency improved with increasing catalyst loading, and the maximum product yield was obtained at 25 mol% of graphene oxide. Further increase in the catalyst amount did not result in any significant improvement in the yield or reduction in reaction time. Therefore, 25 mol% graphene oxide was selected as the optimum catalyst loading and used for all subsequent reactions.

Table 2: Optimization of catalyst for synthesis of Xanthene derivatives.

Entry	Catalyst amount (mol %)	Time (h)	Yield[b](%)
1	No Catalyst	5	00
2	10	4.5	75
3	15	3.4	81
4	20	2.5	84
5	25	2.0	91
6	30	2.0	91

[a]Reaction condition: 3-nitro benzaldehyde (1mmol), ethyl, β-naphthol (1mmol), dimedone (1mmol) in ethanol using different amount of Graphene Oxide at reflux. [b]Isolated Yield After establishing ethanol as the preferred reaction medium and 25 mol% graphene oxide as the optimum catalyst loading, the influence of temperature on the model reaction was investigated. The reaction of β-naphthol (1 mmol), dimedone (1 mmol), and 3-nitro benzaldehyde (1 mmol) was performed at different temperatures while maintaining all other reaction parameters constant (Table 3). The results showed that increasing the reaction temperature improved the conversion and reduced the reaction time. The best result was obtained under refluxing conditions in ethanol,

affording the desired xanthene derivative in the highest yield within the shortest reaction time. Therefore, reflux temperature was selected as the optimum reaction condition for the subsequent substrate scope studies.

Table 3: Effect of temperature on the synthesis of Xanthene derivatives.

Entry	Reaction Temperature (^{o}C)	Time (h)	Yield [b](%)
1	R.T.	5.0	42
2	40	4.0	72
3	50	3.5	80
4	60	2.3	85
5	Reflux	2.0	91

[a]Reaction condition: 3-nitro benzaldehyde (1mmol), ethyl, β-naphthol (1mmol), dimedone (1mmol) in ethanol using 25 mol% of Graphene Oxide at different temperature. [b]Isolated Yield To evaluate the generality and substrate compatibility of the developed protocol, a series of substituted aromatic aldehydes was reacted with β-naphthol and dimedone under the optimized conditions using 25 mol% graphene oxide in ethanol at reflux. As summarized in Table 4, the reaction proceeded smoothly with aromatic aldehydes, affording the corresponding xanthene derivatives in good to excellent yields (82–91%) within 2–3.5 h. The results revealed a clear influence of the electronic nature of the aldehyde substituents on the reaction outcome. Aldehydes bearing electron-withdrawing groups generally showed higher reactivity and furnished the corresponding products in excellent yields. For example, 3-nitrobenzaldehyde afforded the highest yield (91%), whereas 4-fluorobenzaldehyde gave the corresponding product in 88% yield. In contrast, aromatic aldehydes containing electron-donating substituents generally required longer reaction times and afforded comparatively lower yields. The methoxy-substituted substrates gave products in 82% yields after 3.5 h. The enhanced reactivity of electron-deficient aldehydes may be attributed to the increased electrophilicity of the carbonyl carbon, which facilitates the key condensation steps involved in the multicomponent transformation. Overall, these results demonstrate that the graphene oxide-catalyzed protocol exhibits broad substrate tolerance and provides an efficient approach for the synthesis of structurally diverse xanthene derivatives.

Table 4: Synthesis of 2-amino Xanthene derivatives by using Graphene Oxide.

Entry	R	Product	Time (Hr)[a]	Yields (%)
1	4-$CH_3OC_6H_5$	4a	3.5	82
2	3-$NO_2C_6H_5$	4b	2	91
3	4-FC_6H_5	4c	3	88

[a]Yields refer to those of pure isolated products characterized by IR, ^{1}H NMR, and ^{13}C NMR spectroscopic data. The reusability of graphene oxide was investigated using the model reaction of β-naphthol, dimedone, and 3-nitrobenzaldehyde under the optimized reaction conditions. After completion of the reaction, the heterogeneous graphene oxide catalyst was recovered from the reaction mixture by filtration, washed thoroughly with ethanol, dried, and reused in subsequent reaction cycles. The recovered catalyst was evaluated over four cycle consecutive runs. As summarized in Table 5, no significant decrease in product yield was observed during the recycling experiments, demonstrating that graphene oxide retained its catalytic activity upon reuse. These results highlight the practical advantages of graphene oxide as a recoverable and reusable heterogeneous catalyst and further support the sustainability of the developed synthetic protocol.

Table 5: Synthesis of Xanthene (Model reaction) derivatives by using recycled Graphene Oxide.

Entry	Cycle	Time(Hr)	[a]Yield(%)
1	1st Run	2	91
2	2nd Run	2	88
3	3rd Run	2	86
4	4th Run	2	80

[a]Isolated yields

Spectral analysis of representative compounds

1] 9,9-Dimethyl-9,10-dihydro-12-(4-methoxyphenyl)-8*H*benzo[*a*]xanthen-11(12*H*)-one (4a):

^{1}H NMR (300 MHz, $CDCl_3$): 1.22 (s, 6H), 1.98 (s, 2H), 2.72 (s, 2H), 3.53 (s, 3H), 5.63 (s, 1H), 6.70 (d, 2H), 7.20-7.52 (m, 6H), 7.68-7.72 (m, 2H). ^{13}C NMR (300 MHz, $CDCl_3$): δ 27.6, 30.7, 33.2, 41.1, 49.9, 54.5, 112.8, 114.2, 116.8, 120.4, 123.2, 125.0, 126.2, 127.8, 128.5, 130.4, 133.6, 136.2, 145.1, 154.2, 164.0, 192.4.

Mass (GC/MS): *m/z* 385 (M+).

Elemental analysis (%) for $C_{26}H_{24}O_3$: C, 81.22; H, 6.29; Found: C, 81.28; H, 6.21

2] 9,9-Dimethyl-9,10-dihydro-12-(3-nitrophenyl)-8*H*-benzo-[*a*]xanthen-11(12*H*)-one (4b):

^{1}H NMR (300 MHz, $CDCl_3$):δ 1.20 (s, 6H), 2.29 (s, 2H), 2.51 (s, 2H), 5.62 (s, 1H), 7.47- 7.59 (m, 4H), 7.78-7.92 (m, 4H), 8.02-8.09 (m, 2H).

^{13}C NMR (300 MHz, $CDCl_3$): δ 27.2, 30.5, 37.0, 43.2, 52.1, 110.2, 113.9, 118.2, 122.2, 123.5, 124.2, 125.9, 127.7, 128.8, 129.7, 130.6, 131.2, 133.2, 136.0, 145.4, 146.8, 149.2, 163.8, 196.0. Mass (GC/MS): *m/z* 399 (M+).

Elemental analysis (%) for $C_{25}H_{21}NO_4$: C, 75.17; H, 5.30; N, 3.51. Found: C, 75.26; H, 5.41; N, 3.66.

3] 12-(4-Fluorophenyl)-9,9-dimethyl-8,9,10,12-tetrahydrobenzo[*a*]xanthen-11-one (4c):

^{1}H NMR (300 MHz, $CDCl_3$): δ 1.24 (s, 6H), 2.18 (s, 2H), 2.78 (s, 2H), 5.75 (s, 1H), 6.30 (m, 2H), 7.27-7.43 (m, 6H), 7.75 (m, 2H).

^{13}C NMR (300 MHz, $CDCl_3$): δ 27.8, 32.9, 37.2, 41.5, 52.4, 112.4, 114.9, 116.4, 118.8, 119.6, 122.8, 125.2, 127.8, 128.8, 129.8, 130.7, 131.5, 134.2, 144.3, 148.8, 165.1, 194.6.

Mass (GC/MS): *m/z* 372 (M+).

Elemental analysis (%) for $C_{25}H_{21}O_2F$: C, 80.62; H, 5.68. Found: C, 80.45; H, 5.82.

4.1. Molecular docking studies

Molecular docking analysis was performed to investigate the binding behavior of the synthesized benzo[a]xanthene derivatives and to characterize their predicted interactions within the selected protein binding pocket. Docking calculations were carried out using AutoDock Vina. The receptor was used in prepared PDBQT format as 4WKQ.pdbqt. The center of the docking grid was set at (x = 9.927), (y = 201.795), and (z = 23.020) Å, while the dimensions of the search space were 66 × 46 × 52 Å along the x-, y-, and z-axes, respectively. The exhaustiveness parameter was set to 10.

The docking poses were subsequently evaluated on the basis of the predicted binding affinity and the amino acid residues reported to interact with each ligand. The analysis focused on the reported hydrogen-bond interactions, hydrogen-bond distances, and additional hydrophobic or other residue contacts.

4.2. Docking results and interaction analysis

Three benzo[a]xanthene derivatives were examined: 9,10-dihydro-12-(4-methoxyphenyl)-9,9-dimethyl-8H-benzo[a]xanthen-11(12H)-one (1A), 9,10-dihydro-9,9-dimethyl-12-(3-nitrophenyl)-8H-benzo[a]xanthen-11(12H)-one (1B), and 12-(4-fluorophenyl)-9,10-dihydro-9,9-dimethyl-8H-benzo[a]xanthen-11(12H)-one (1C). The predicted binding affinities obtained from the docking analysis were −8.8, −8.8, and −8.6 kcal mol^{-1} for compounds 1A, 1B, and 1C, respectively as summarized in **Table 5.**

Table 5: Predicted binding affinities and protein–ligand interactions of benzo[a]xanthene derivatives 1A–1C.

Product	Binding Affinity (Kcal/mol)	Hydrogen Bond Interaction	Hydrogen Bond Length in A^0	Hydrophobic & other Interaction
1A	-8.8	LEU-798	3.25	LEU-799, ARG-841, LEU-718, ALA-743, LEU-844, VAL-726
1B	-8.8	SER-912, THR-909	2.37, 3.35	PHE-910, ILE-938, PRO-937
1C	-8.6	TYR-915, SER-912	2.43, 3.38	PRO-934

Compound 1A, bearing a 4-methoxyphenyl substituent, also exhibited a predicted binding affinity of −8.8 kcal mol^{-1}. LEU-798 was reported as the hydrogen-bonding residue, with an interaction distance of 3.25 Å. Additional interactions were reported with LEU-799, ARG-841, LEU-718, ALA-743, LEU-844, and VAL-726. Thus, compound 1A displayed a distinct residue-interaction pattern compared with compounds 1C and 1B, despite having the same predicted binding affinity as compound 1B. Compound 1B, containing a 3-nitrophenyl substituent, showed a predicted binding affinity of −8.8 kcal mol^{-1}. Hydrogen-bond interactions were reported with SER-912 and THR-909, with distances of 2.37 and 3.35 Å, respectively. PHE-910, ILE-938, and PRO-937 were additionally reported as residues involved in hydrophobic and other interactions. The interaction pattern therefore differs from that observed for compound 1C, with SER-912 retained as a common reported residue while additional contacts were observed with THR-909, PHE-910, ILE-938, and PRO-937. Compound 1C, bearing a 4-fluorophenyl substituent, exhibited a predicted binding affinity of −8.6 kcal mol^{-1}. The interaction analysis identified TYR-915 and SER-912 as hydrogen-bonding residues, with reported interaction distances of 2.43 and 3.38 Å, respectively. PRO-934 was additionally reported among the hydrophobic and other interactions. These contacts indicate that the predicted binding pose of 1C is associated with both polar interactions and additional contacts with residues surrounding the binding region.

The predicted binding orientations of the three benzo[a]xanthene derivatives and their corresponding protein–ligand interaction profiles are presented in Fig. 4, 5 & 6 respectively. The three-dimensional poses illustrate the positioning of each ligand within the binding pocket, while the corresponding two-dimensional diagrams provide a residue-level

representation of the reported intermolecular interactions.

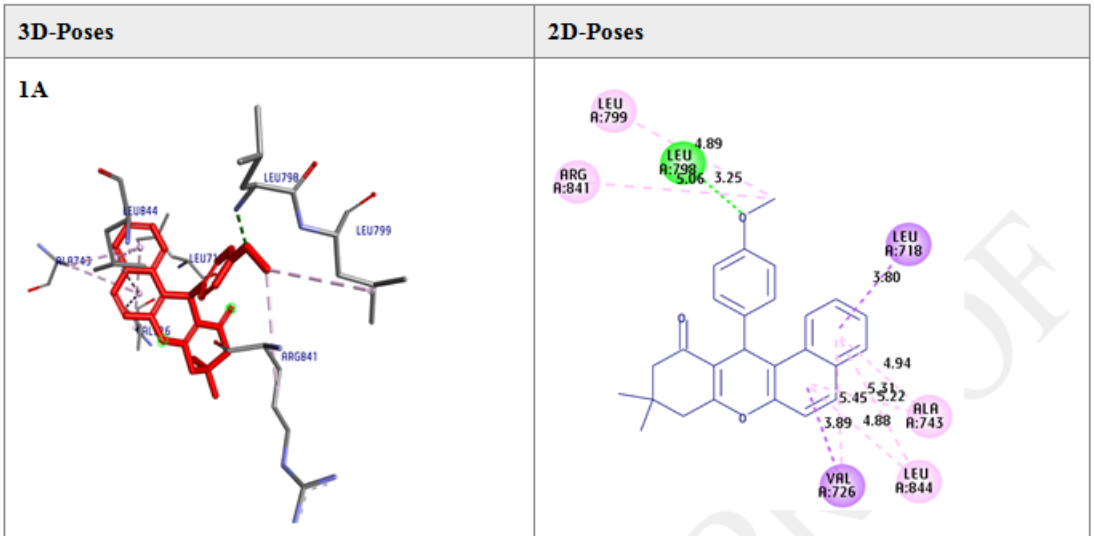

Fig 4: 3-D molecular docking pose and corresponding 2-D protein–ligand interaction of 1A.

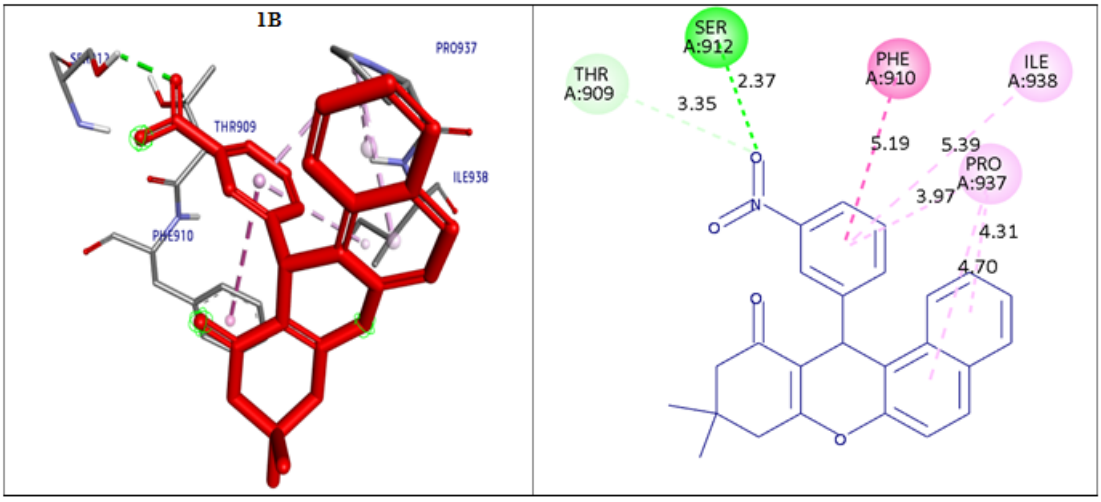

Fig 5: 3-D molecular docking pose and corresponding 2-D protein–ligand interaction of 1B

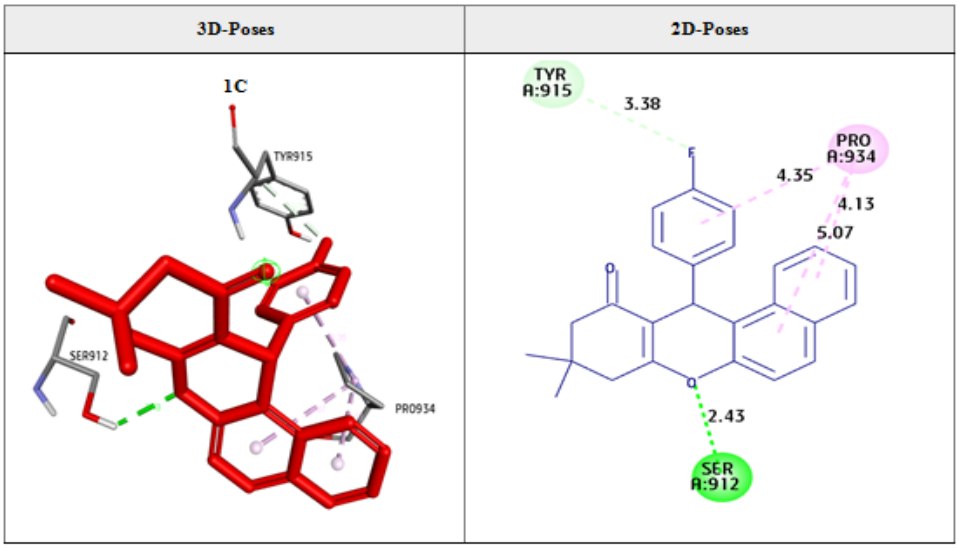

Fig 6: 3-D molecular docking pose and corresponding 2-D protein–ligand interaction of 1C.

4.3. Comparative discussion

The docking results showed relatively similar predicted binding affinities for the three derivatives, ranging from −8.6 to −8.8 kcal mol⁻¹. Compounds 1A and 1B produced identical predicted binding affinities of −8.8 kcal mol⁻¹, whereas compound 1C gave a value of −8.6 kcal mol⁻¹. Thus, within the scoring results obtained under the present docking conditions, compounds 1A and 1B have the same reported docking score, while the difference between 1C and the other two derivatives is 0.2 kcal mol⁻¹. These numerical differences should be interpreted cautiously and should not be equated directly with experimentally determined differences in binding affinity.

The residue-level interaction data demonstrate that the three derivatives adopt different predicted interaction patterns within the binding pocket. Compound 1C showed reported interactions with TYR-915, SER-912, and PRO-934, whereas compound 1B interacted with SER-912, THR-909, PHE-910, ILE-938, and PRO-937. Compound 1A showed contacts with LEU-798, LEU-799, ARG-841, LEU-718, ALA-743, LEU-844, and VAL-726. These differences indicate that modification of the phenyl-ring substituent is accompanied by changes in the reported residue-contact profile of the docked molecules.

The hydrogen-bond distances reported for compounds 1C and 1B were 2.43 and 3.38 Å and 2.37 and 3.35 Å, respectively, while the reported distance for the LEU-798 interaction of 1A was 3.25 Å. These distances are reported as obtained from the docking analysis. The precise chemical nature and geometry of each interaction should be interpreted together with the corresponding docking poses or two-dimensional interaction diagrams rather than from distance alone.

Taken together, the docking analysis provides a comparative structural description of the predicted binding modes of the three synthesized derivatives. All three compounds showed favorable negative docking scores under the applied AutoDock Vina protocol, with values of −8.6 to −8.8 kcal mol⁻¹. The results also revealed distinct residue-interaction patterns for the methoxy-, nitro-, and fluoro-substituted derivatives.

5. CONCLUSION

In conclusion, an efficient and greener protocol for the one-pot synthesis of xanthene derivatives has been developed through the three-component reaction of β-naphthol, dimedone, and aromatic aldehydes using graphene oxide as a heterogeneous catalyst in ethanol under reflux conditions. The methodology affords the desired products in good to excellent yields with broad substrate applicability and straightforward work-up. The use of graphene oxide as a metal-free, heterogeneous, and potentially recyclable catalyst, together with ethanol as a comparatively benign reaction medium, enhances the practical and environmental appeal of the protocol. Thus, the present approach provides a simple, efficient, and sustainable alternative for the synthesis of structurally diverse xanthene derivatives. Molecular docking studies provided preliminary insights into the predicted protein–ligand interactions of the selected synthesized xanthene derivatives. The compounds exhibited predicted binding affinities ranging from −8.6 to −8.8 kcal mol⁻¹, with distinct hydrogen-bonding and additional residue interaction profiles within the selected binding pocket. These computational findings complement the experimental results and provide a basis for further investigation of the biological potential of the synthesized derivatives.

ACKNOWLEDGMENT

The authors gratefully acknowledge Principal Yogeshwari Mahavidyalaya, Ambajogai, Maharashtra, India, for providing laboratory facilities and essential research infrastructure necessary to carry out this work. The authors also express their sincere appreciation to the Department of Chemistry for its continuous support during the course of this investigation.

REFERENCES

1. Hideo, T.; Teruomi, J. 1-Benzopyrano[2,3-b]xanthene Derivative and Its Preparation. Jpn. Patent 56005480, 1981.
2. Kidwai, M.; Jahan, A.; Mishra, N. K. A novel method for the synthesis of tetrahydrobenzo[a]-xanthen-11-one derivatives using cerium(III) chloride as a highly efficient catalyst. C. R. Chim., 2012; 15: 324–330. DOI: 10.1016/j.crci.2012.01.002.
3. Lambert, R. W.; Martin, J. A.; Merrett, J. H.; Parkes, K. E. B.; Thomas, G. J. Pyrimidine Nucleosides. PCT Int., Appl. WO 9706178, 1997.
4. Knight, C. G.; Stephens, T. Xanthene-dye-labelled phosphatidylethanolamines as probes of interfacial pH. Studies in phospholipid vesicles. Biochem. J., 1989; 258: 683–687. DOI: 10.1042/bj2580683.
5. Banerjee, A.; Mukherjee, A. K. Chemical aspects of santalin as a histological stain. Stain Technol., 1981; 56: 83–85. DOI: 10.3109/10520298109067286.
6. Menchen, S. M.; Benson, S. C.; Lam, J. Y. L.; Zhen, W.; Sun, D.; Rosenblum, B. B.; Khan, S. H.; Taing, M. Sulfonated diarylrhodamine dyes. U.S. Patent, 2003; 6(583): 168 B1.
7. Kumar, A.; Rout, L.; Achary, L. S. K.; Dhaka, R. S.; Dash, P. Greener route for synthesis of aryl and alkyl-14H-dibenzo[a,j]xanthenes using graphene oxide-copper ferrite nanocomposite as a recyclable heterogeneous catalyst. Sci. Rep., 2017; 7: 42975. DOI: 10.1038/srep42975.
8. Ahmad, M.; King, T. A.; Ko, D.-K.; Cha, B. H.; Lee, J. Performance and photostability of xanthene and pyrromethene laser dyes in sol-gel phases. J. Phys. D: Appl. Phys., 2002; 35: 1473–1476. DOI: 10.1088/0022-3727/35/13/303.
9. Wang, R.-Z.; Zhang, L.-F.; Cui, Z.-S. Iodine-catalyzed synthesis of 12-aryl-8,9,10,12-

tetrahydrobenzo[a]xanthen-11-one derivatives via multicomponent reaction. Synth. Commun., 2009; 39: 2101–2107. DOI: 10.1080/00397910802638511.
10. Sadeghpour, M.; Olyaei, A.; Rezaei, M. Guanidine hydrochloride: A highly efficient organocatalyst for the synthesis of 12-aryl-8,9,10,12-tetrahydrobenzo[a]xanthene-11-ones under solvent-free conditions. J. Heterocycl. Chem., 2016; 53: 981–988. DOI: 10.1002/jhet.1879.
11. Karimi, N.; Oskooie, H. A.; Heravi, M. M.; Tahershamsi, L. Caro's acid-silica gel-catalyzed one-pot synthesis of 12-aryl-8,9,10,12-tetrahydrobenzo[a]xanthen-11-ones. Synth. Commun., 2011; 41: 307–312. DOI: 10.1080/00397910903537372.
12. Mo, L.-P.; Chen, H.-L. One-pot, three-component condensation of aldehydes, 2-naphthol and 1,3-dicarbonyl compounds. J. Chin. Chem. Soc., 2010; 57: 157–161. DOI: 10.1002/jccs.201000025.
13. Wang, H.-J.; Ren, X.-Q.; Zhang, Y.-Y.; Zhang, Z.-H. Synthesis of 12-aryl or 12-alkyl-8,9,10,12-tetrahydrobenzo[a]xanthen-11-one derivatives catalyzed by dodecatungstophosphoric acid. J. Braz. Chem. Soc., 2009; 20: 1939–1943. DOI: 10.1590/S0103-50532009001000025.
14. Zhang, Z.-H.; Zhang, P.; Yang, S.-H.; Wang, H.-J.; Deng, J. Multicomponent, solvent-free synthesis of 12-aryl-8,9,10,12-tetrahydrobenzo[a]xanthen-11-one derivatives catalyzed by cyanuric chloride. J. Chem. Sci., 2010; 122: 427–432. DOI: 10.1007/s12039-010-0049-0.
15. Nandi, G. C.; Samai, S.; Kumar, R.; Singh, M. S. An efficient one-pot synthesis of tetrahydrobenzo[a]xanthen-11-one and diazabenzo[a]anthracene-9,11-dione derivatives under solvent-free condition. Tetrahedron, 2009; 65: 7129–7134. DOI: 10.1016/j.tet.2009.06.024.
16. Li, J.; Tang, W.; Lu, L.; Su, W. Strontium triflate-catalyzed one-pot condensation of β-naphthol, aldehydes and cyclic 1,3-dicarbonyl compounds. Tetrahedron Lett., 2008; 49: 7117–7120. DOI: 10.1016/j.tetlet.2008.09.129.
17. Shinde, P. V.; Kategaonkar, A. H.; Shingate, B. B.; Shingare, M. S. Surfactant catalyzed convenient and greener synthesis of tetrahydrobenzo[a]xanthene-11-ones at ambient temperature. Beilstein J. Org. Chem., 2011; 7: 53–58. DOI: 10.3762/bjoc.7.9
18. Zare, A.; Mokhlesi, M.; Hasaninejad, A.; Hekmat-Zadeh, T. Solvent-free synthesis of 1,8-dioxo-octahydroxanthenes and 14-aryl-14H-dibenzo[a,j]xanthenes using saccharin sulfonic acid as an efficient and green catalyst. E-J. Chem., 2012; 9: 1854–1863. DOI: 10.1155/2012/596862.
19. Hassankhani, A.; Mosaddegh, E.; Ebrahimipour, S. Y. H4SiW12O40-catalyzed one-pot synthesis of 12-aryl-8,9,10,12-tetrahydrobenzo[a]xanthen-11-ones under solvent-free conditions. E-J. Chem., 2012; 9: 786–790. DOI: 10.1155/2012/930251.
20. Anjali; Mishra, A.; Khurana, M.; Pani, B.; Awasthi, S. K. Recent advances in functionalization of graphene oxide and its role in catalytic organic transformations: A comprehensive review (2018–2024). ChemistrySelect, 2025; 10: e202404742. DOI: 10.1002/slct.202404742.
21. Nishina, Y. Mass production of graphene oxide beyond the laboratory: Bridging the gap between academic research and industry. ACS Nano 2024, 18, 33264–33275. DOI: 10.1021/acsnano.4c13297 Dreyer, D. R.; Park, S.; Bielawski, C. W.; Ruoff, R. S. The chemistry of graphene oxide. Chem. Soc. Rev., 2010; 39: 228–240. DOI: 10.1039/B917103G.
22. Dreyer, D. R.; Jia, H.-P.; Bielawski, C. W. Graphene oxide: A convenient carbocatalyst for facilitating oxidation and hydration reactions. Angew. Chem. Int. Ed., 2010; 49: 6813–6816. DOI: 10.1002/anie.201002160.